Birefringence and reflectivity of single-crystal $CdAl_2Se_4$ by generalized ellipsometry

J.-D. Hecht,* A. Eifler, and V. Riede
Faculty of Physics and Geoscience, Department of Solid State Optics, University of Leipzig, Linnéstraße 5, D-04103 Leipzig, Germany

M. Schubert
Faculty of Physics and Geoscience, Department of Semiconductor Physics, University of Leipzig, Linnéstraße 5, D-04103 Leipzig, Germany

G. Krauß and V. Krämer
Freiburg Center for Materials Science, Albert-Ludwigs-University, Stefan-Meyer-Straße 21, D-79104 Freiburg, Germany
(Received 8 September 1997; revised manuscript received 14 November 1997)

Transmission and reflection generalized variable-angle spectroscopic ellipsometry and polarized transmission intensity measurements over the photon energy range from 0.74 to 5.0 eV have been used to characterize the optical properties of the ordered-vacancy compound $CdAl_2Se_4$. We report the dispersion of the uniaxial refractive index below the band gap. The onset of weak absorption indicates the fundamental band edge at about 2.95 eV, but does not reveal the nature of the lowest band-to-band transition. Above the fundamental band gap we assign four possible critical-point structures from a line-shape analysis of the sample dielectric function. [S0163-1829(98)06812-X]

I. INTRODUCTION

Because of their large potential for technological applications (e.g., photovoltaic and nonlinear optical devices) most of the chalcopyrite and related ordered-vacancy compounds (OVC's) have been thoroughly investigated.[1–4] Due to difficulties with crystal growth and sample preparation of the $A^{II}B_2^{III}C_4^{VI}$ OVC's with B^{III}=Al, such as the high oxygen affinity of aluminum, only very little is known about the physical properties of these OVC's. Very recently, high-purity crystals of $CdAl_2Se_4$ were grown by the chemical vapor transport technique.[5] $CdAl_2Se_4$ crystallizes in the thiogallate structure (uniaxial, space group $I\bar{4}$, Fig. 1), and anisotropic optical properties should be expected. In this paper we report angular-resolved generalized anisotropic ellipsometry investigations over the photon energy range from 0.74 to 5 eV to determine the optical properties of uniaxial single crystal $CdAl_2Se_4$ samples grown by Krauß *et al.*[5]

Band-structure calculations for the $A^{II}B_2^{III}C_4^{VI}$ compounds with A^{II}=Cd, Zn, B^{III}=In, and C^{VI}=Se, Te when crystallized in tetrahedral arrangement (space group $P\bar{4}2m$) predicted the fundamental band edge E_0 as an indirect band-to-band transition, and the lowest direct interband transition about 200 meV above the fundamental edge.[6] All compounds should be very similar in their band structures, which themselves are similar to those of the compound zinc-blende analogs.[6,7] The upper valence band was found to be very flat, and the nature of E_0 needs experimental verification.[8] For $CdGa_2Se_4$ (space group $I\bar{4}$) MacKinnon also predicted an indirect band gap that involves a transition from the Brillouin-zone X-point valence-band maximum to the Γ-point conduction-band minimum.[8] Bernard and Zunger predicted a direct nature for the band gap of α-$CdIn_2Se_4$ (space group $P\bar{4}2m$).[9]

Trykozko and Huffman observed five critical points in partially disordered $CdIn_2Se_4$ including E_0 from unpolarized synchrotron-radiation reflectivity data in the photon energy (E) range $1.5 \leqslant E \leqslant 6.5$ eV.[10] Using the results from band-structure calculations reported by Baldereschi *et al.*,[6] the authors assigned the critical-point structures to direct interband transitions, i.e., E_0 (1.75 eV) as Γ-Γ, E_1 (3.7 eV) and E_2 (4.3 eV) as R-R, E_3 (5.4 eV), as Γ-Γ, and E_4 (6.3 eV) as a sum of M-M and X-X transitions. They also noted that the E_1 structure is similar to the E_1 critical-point behavior in binary zinc-blende compounds. As well, E_4 was assigned as a feature due to M_1 and M_2 critical points known as the E_2 critical point in III–V compounds. Trykozko and Huffman further noted the existence of a spin-orbit splitting at the lowest Brillouin-zone-center transition ($E_0+\Delta_0$).

Syrbu and Tezlevan investigated the OVC's $CdGa_2Se_4$ and $CdAl_2S_4$ using polarized reflection measurements.[11] A

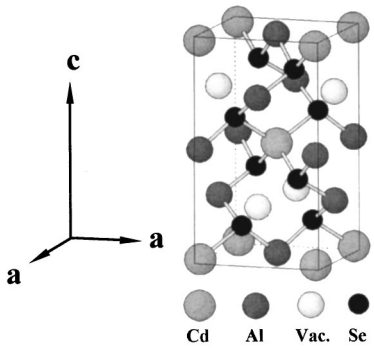

FIG. 1. Crystal structure of the uniaxial defect chalcopyrite $CdAl_2Se_4$ (thiogallate structure, $I\bar{4}$). The ordered-vacancy compound is a derivative of the centered tetragonal ternary $A_nB_{4-n}C_4$ chalcopyrite compounds ($I\bar{4}2d$, see, e.g., Bernard and Zunger, Ref. 9).

strong dependence of the reflectance critical-point structures on the incident light polarization direction was observed. A total of seven critical points (including their spin-orbit split partners within the photon energy range from 1 to 6 eV) were assigned.

For $CdAl_2Se_4$, no experimental data have been reported so far. Only the fundamental band gap has been presented by Krauß *et al.* Assuming a direct interband transition, E_0 was obtained from unpolarized absorption measurements at 2.95 eV.[5]

Ellipsometry is known as a fast, nondestructive, and precise optical technique that determines the complex reflectance ratio $\rho = R_p/R_s$ of samples with plane parallel boundaries, where R_p and R_s are the complex reflectance coefficients of p- and s-polarized light, respectively.[12] Generalized variable-angle of incidence spectroscopic ellipsometry (gVASE) takes into account sample optical anisotropy and detects ''p'' and ''s''-wave conversions. The extension of rotating-analyzer ellipsometry, a standard ellipsometry technique, to gVASE capabilities has been reported recently, and demonstrated through applications to birefringent layered media.[13–16] The basis of gVASE is to measure normalized *complex* ratios involving all four elements of the 2×2 Jones matrix describing the sample.[12] These normalized Jones-matrix elements may be measured in transmission (T_{pp}, T_{ps}, and T_{sp}), or reflection (R_{pp}, R_{ps}, and R_{sp}) arrangement. Note that in cases where no ''p''- and ''s''-wave conversions occur, the ratios T_{pp} and R_{pp} are identical to the standard transmission and reflection ellipsometric parameters. Polarized transmission intensity (PTI) measurements allow for determination of aligned (diagonal, i.e., $|t_{pp}|^2$, and $|t_{ss}|^2$) or crossed (off-diagonal, i.e., $|t_{ps}|^2$, and $|t_{sp}|^2$) polarized modulus-squared Jones-matrix elements. For a definition of the Jones matrix and the framework of the coordinate system used in this work, we refer the reader to Refs. 12–18. In order to analyze the gVASE and PTI data, one needs to model the sample structure together with the optical properties of the materials involved. The measured data are then subject to a regression procedure that involves a 4×4 matrix formalism that accounts for propagation of electromagnetic plane waves through anisotropic materials.[16,18]

For ellipsometric data analysis simple parametric optical constants models such as the Cauchy model for dielectrics[17] or the Zollner model for semiconductor oxides[19] are often utilized.[20] General parametric models that completely describe critical-point structure and line shape of the dielectric function of semiconductors are complex and have been developed, e.g., by Kim *et al.*[21] and Kim, Garland, and Raccah.[22] Such models reveal information about critical-point energies, critical-point broadenings, and the joint density of states. Accurate critical-point energies and linewidths are then obtained from analysis of the dielectric function and its derivatives.[22] However, to ensure sufficient accuracy the numerical differentiation of ellipsometric data requires attention because differentiating optical data may distort real spectral features.[23] A simple method to eliminate systematic distortions and broadenings introduced by numerical differentiation has been proposed by Garland *et al.*[23] employing a Savitzky-Golay[24] algorithm. However, for this work we make use of a less ambitious parametric optical constants model, a three-dimensional M_1 critical-point structure based on the parabolic band approximation and an oscillator ensemble, to model the semiconductor critical-point structure above the fundamental band gap.[25] Analysis of the sample dielectric function and its second derivative is then performed simultaneously. However, we did not explicitly fit the second derivative. We used the criterion that the model second derivative matches the experimental second derivative as a supplementary condition for having a good fit to the ellipsometric data. The numerical derivative is obtained by locally fitting a polynomial to the ellipsometric data.[26]

For optical investigations on anisotropic samples it is necessary to specify the in-plane orientation φ of the sample with respect to the plane of incidence (e.g., Fig. 2 in Ref. 13). We define the sample azimuth φ as the angle between the x axis of our laboratory coordinate system (see Fig. 1 in Ref. 16 where the x axis is parallel to the plane of incidence), and the projection of the optical axis (which is parallel to the sample c axis, Fig. 1) through to the sample surface. The Euler angles φ, ψ, and θ (Fig. 2 in Ref. 14) are then associated with the respective crystal coordinate system during measurement, and provide the orthogonal rotation matrices that diagonalize the dielectric tensor that is given in laboratory coordinates.[16] For our $CdAl_2Se_4$ sample the Euler angles φ and θ are the azimuth and the inclination angles of the optical axis with respect to the x and z axes, respectively, whereas ψ is equal to 0°. Note that the Euler angle φ is the same as the sample azimuth defined above.

II. EXPERIMENT

A $CdAl_2Se_4$ single crystal was grown by the chemical vapor transport method.[5] The thiogallate structure was confirmed by x-ray investigation (Rietveld method).[5] The lattice constants were determined to be $a = 5.7606$ Å and $c = 10.7138$ Å.[5] The crystal was unoriented sliced and polished on both sides with 50-nm corundum. The sample size is $4\times4\times0.32$ mm^3 as determined from caliper measurements.

Generalized VASE measurements were carried out in transmission at two 45°-like sample azimuth orientations. (these angles were later determined from the sample best fit as $\varphi = -45°$ and $-135°$), and at multiple angles of incidence ($\Phi_a = -30°$, $-15°$, 0°, 15°, and 30°) for photon energies from 0.74 to 3 eV. In addition, PTI measurements for both aligned and crossed polarizer for p-polarized input light were performed at the same sample setup, and incident light conditions. Reflection-type gVASE data were taken at multiple sample azimuths ($0° \leqslant \varphi \leqslant 360°$), and incident photon energies from 3 to 5 eV. As well, at $E = 1.5$ eV reflection-type gVASE data were measured as a function of incidence angle ($30° \leqslant \Phi_a \leqslant 75°$) at $\varphi = -45°$ and $-135°$. This work was done with a commercial spectroscopic rotating-analyzer ellipsometer with automated compensator (J. A. Woollam Co.). The automated compensator allows for complete determination of the phase Δ of the polarization state ($0° \leqslant \Delta \leqslant 360°$) of the light wave emerging from the sample. The same equipment was used for PTI data acquisition.

III. RESULTS AND DISCUSSION

Depending on the spectral range and the acquisition mode during our optical investigations, i.e., according to the pen-

etration depth of the electromagnetic light waves into the sample, the experimental data information refer to bulk- or surface-related sample properties. Our transmission-type data are mainly influenced by the bulk refractive indices, and surface-related effects are negligible. A single-layer model was used for their analysis.

The reflection-type data acquired above E_0 contain information from the near-surface region only, and are therefore extremely sensitive to any surface overlayer. The latter usually complicates the accurate determination of bulk refractive indices. If bulk-related critical-point contributions to ϵ, the dielectric function of the bulk material, are of interest one can avoid the exact treatment of surface overlayer effects by using the pseudodielectric function $\langle\epsilon\rangle$ as target data for the sample regression analysis. The pseudodielectric function is a representation of the standard isotropic ellipsometric parameters Ψ and Δ assuming a two-phase model, and a good approximation to ϵ when the surface overlayer consists of contaminants only.[27] Nevertheless, we used an effective dielectric medium approximation to account for surface roughness, modeling a roughness layer (thickness d_r) by averaging the ambient (air) and bulk ($CdAl_2Se_4$) dielectric functions.[17,28] Note that no contaminants or oxide materials are treated in this concept.

Data within the band-gap spectral region are difficult to analyze due to the gradual change between bulk- and surface-related effects. Decaying multiple reflections within the sample overlap with the typical E_0 structure are usually observable in reflection arrangement on bulk materials. We therefore omit the presentation and discussion of the E_0 spectral range in this work because further investigations on more appropriate samples with smaller thicknesses are necessary.

As an example, Fig. 2 shows experimental (symbols) and calculated (solid lines) gVASE transmission data [$T_{ps}=\tan\Psi_{ps}\exp(i\Delta_{ps})$] in terms of Ψ_{ps} (a), and Δ_{ps} (b) acquired at $\varphi=-45°$. The data type $T_{sp}=\tan\Psi_{sp}\exp(i\Delta_{sp})$ is symmetrical to T_{ps} in that Δ_{sp} differs from Δ_{ps} by a sign only. Due to the 45°-type orientation of the optical axis with respect to the x and y axes, T_{pp} is close to unity. We therefore omit the presentation of T_{sp} and T_{pp} here. For a more detailed discussion of the properties of anisotropic samples and their Jones-matrix representation we refer the reader to Refs. 13–18.

Figure 3 depicts the modulus-squared Jones-matrix elements $|t_{ps}|^2$ (a) and $|t_{pp}|^2$ (b) obtained from crossed and aligned polarizer PTI measurements at $\varphi=-135°$. Note that the data shown in Figs. 2 and 3 are related in that T_{ps} is the complex ratio t_{ps}/t_{pp}. The change in period and amplitude in Ψ_{ps}, Δ_{ps}, $|t_{ps}|^2$, and $|t_{pp}|^2$ by varying the angle of incidence is due to different propagation directions of the electromagnetic plane waves relative to the major crystal axes. Note that the gVASE transmission data are highly sensitive to the major axis orientations and major refractive index differences, whereas the PTI and gVASE reflection data at $E=1.5$ eV (not shown here) contain necessary information about the absolute refractive index values.

The data in Figs. 2 and 3 reveal the $CdAl_2Se_4$ birefringence in the below-gap spectral range. At this point we emphasize generalized ellipsometry as an appropriate technique to investigate the optical anisotropies of noncubic OVC's.

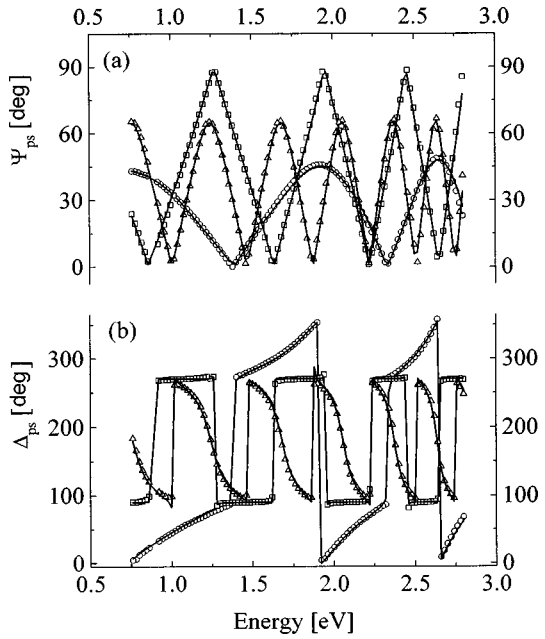

FIG. 2. Experimental data (symbols) [(a) Ψ_{ps} and (b) Δ_{ps}] for the cross-polarization coefficient $T_{ps}=\tan\Psi_{ps}\exp(i\Delta_{ps})$, as a function of the incident angle Φ_a obtained from transmission gVASE measurements ($\bigcirc$ $\Phi_a=-30°$, $\square$ $\Phi_a=0°$, $\triangle$ $\Phi_a=30°$; sample azimuth $\varphi=-45°$). The best fit (solid lines) for n_o, n_e, the sample thickness d, and the Euler angles of the optical axis φ, and θ is obtained by simultaneous analysis of multiple-angle-of-incidence and multiple-sample-azimuth reflection- and transmission-type data from the spectral region below the band gap. The optical axis is tilted from the sample normal by $\theta=-61°$. The sample azimuth is $\varphi=-45°$. Note the change of period and amplitude in Ψ_{ps} with varying angle of incidence due to different orientations of the major crystal axes with respect to the ellipsometric coordinate system.

The calculated data in Figs. 2 and 3 were obtained from a multiple-data-type regression analysis for the sample optical (major refractive indices) and structural (thickness, major crystal axis orientations) properties involving the gVASE and PTI data acquired at multiple angles of incidence and sample orientations. For sample analysis a 4×4 matrix formalism that accounts for plane-wave propagation through anisotropic layers (with an extension to allow for transmission through anisotropic substrates) has been used.[18] Note that the optical characterization of an anisotropic layer is a challenge when the thickness exceeds the incident light wavelength by order of magnitudes. The presence of multiple discrete polarization states due to the finite coherence length of the light source results in partial depolarization of the light beam emerging from the sample. Multiple beams are generated by multiple reflections between the front and the back surfaces. In order to model the detected data types we assume that a single beam consisting of two copropagating eigenstates maintains internal coherence, whereas different beams are treated as incoherent.[18]

We have parametrized the major below-gap refractive indices n_e (electric field polarization $E\|c$), and n_o ($E\perp c$) of $CdAl_2Se_4$ through a Cauchy dispersion model (Table I). We obtain that $CdAl_2Se_4$ is uniaxial negative below the band gap ($n_e<n_o$), and no crossover (isotropy point) occurs (Fig. 4). The major refractive index differences remain nearly con-

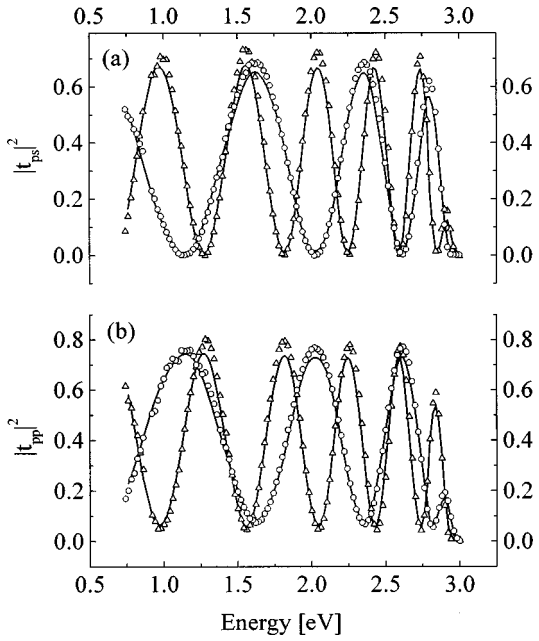

FIG. 3. Same as Fig. 2 for the modulus-squared Jones-matrix elements $|t_{ps}|^2$ (a) and $|t_{pp}|^2$ (b) ($\triangle$ $\Phi_a=-15°$, $\bigcirc$ $\Phi_a=15°$; sample azimuth $\varphi=-135°$). The experimental data were obtained from angle-resolved crossed and aligned PTI measurements for p-polarized incident light. The calculated data (solid lines) were obtained from the same best fit as shown in Fig. 2. Whereas the gVASE transmission data are highly sensitive to the major axis orientations and the major refractive index differences, the polarized transmission intensities reveal the absolute refractive index values. Note the onset of absorption above $\sim$2.8 eV where both $|t_{ps}|^2$ and $|t_{pp}|^2$ begin to vanish.

stant ($n_o-n_e\sim0.02$), since both n_e, and n_o show the same dispersion. We further obtained the inclination angle of the sample c axis as $\theta=-(61\pm0.1)°$. The azimuth angles that determine the in-plane orientation of the sample during data acquisition were found as $\varphi=-(45\pm0.1)°$ and $-(135\pm0.1)°$, respectively. The best-fit sample thickness $d=(320\pm5)$ μm is in agreement with the caliper measurements. The crystal axis orientations were confirmed by polarization microscopy investigations.

From the onset of weak absorption in our PTI data above $\sim$2.8 eV we obtain a very small extinction coefficient k (Fig. 4). A linear extrapolation of the absorption edge implies the existence of E_0 at an energy of $\sim$2.95 eV. However, due to the large thickness of the sample and the few available data points for k we were unable to judge whether this onset of absorption refers to a direct or indirect fundamental band-to-band transition. Furthermore, the PTI data did not provide sufficient sensitivity to distinguish between ordinary and extraordinary absorption coefficients. We therefore treated k as

TABLE I. $CdAl_2Se_4$ below-gap major refractive indices ($n=\alpha+\beta E^2+\gamma E^4$).

	α	β (eV^{-2})	γ (eV^{-4})
$n_o(E\perp c)$	2.283 ± 0.005	$(16.42\pm0.05)10^{-3}$	$(2.21\pm0.1)10^{-3}$
$n_e(E\parallel c)$	2.264 ± 0.005	$(16.12\pm0.05)10^{-3}$	$(2.13\pm0.1)10^{-3}$

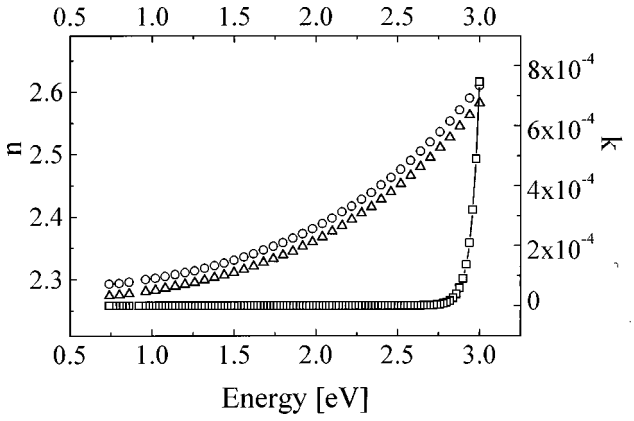

FIG. 4. Major ($\bigcirc$ ordinary n_o, $\triangle$ extraordinary n_e) below-gap refractive indices of $CdAl_2Se_4$ determined from best fit applying a 4×4 matrix formalism and modeling the gVASE and PTI data. As a result we obtain a small extinction coefficient k as well ($\square$). (Note the large thickness $d=320$ μm of the sample compared to the slowly disappearing polarized transmission intensities above $\sim$2.8 eV in Fig. 3.) Note also that our data did not provide enough sensitivity for resolution of different major absorption indices. We therefore treated the extinction coefficient k isotropically.

isotropic. Further investigations of the absorption coefficient within the fundamental band-gap spectral range are necessary for which samples with smaller thicknesses are required.

Figure 5 presents experimental (symbols) and calculated (solid lines) reflection-type gVASE data in terms of the pseudodielectric function $\langle\epsilon\rangle$ (a) and its second derivative $d^2\langle\epsilon\rangle/dE^2$ (b) for photon energies from 3 to 5 eV.[27] At every sample azimuth φ and photon energy E, the $CdAl_2Se_4$ sample surface did not reveal any ''p''- and ''s''-wave conversion, i.e., $R_{ps}=R_{sp}=0$. As well, R_{pp} was independent of φ, thus identical to $\rho=R_p/R_s=\tan\Psi\exp(i\Delta)$, where Ψ and Δ are the standard ellipsometric parameters. We interpret the isotropic reflectivity as being due to the polishing process in which crystallographic defects are incorporated into the near-surface region (some microns in depth). Because of the large absorption above E_0 the reflected light beam information depth is less than the surface region. We therefore observed isotropically averaged $CdAl_2Se_4$ reflectivity data. The gVASE data (R_{pp} only) acquired at multiple sample azimuths were then averaged and converted into $\langle\epsilon\rangle$ eliminating the dependence on Φ_a.[17]

We have analyzed $\langle\epsilon\rangle$ through a detailed line-shape analysis using Adachi's critical-point model for ϵ of semiconductor compound materials.[25,29] In this model, each critical-point structure contributes to the dielectric function. Our line-shape analysis of $\langle\epsilon\rangle$ and its second derivative $d^2\langle\epsilon\rangle/dE^2$ suggested four critical-point structures (E_1-E_4), which are indicated by arrows in Fig. 5. The second derivative was calculated by locally fitting a polynomial to $\langle\epsilon\rangle$.[26] The second-degree fitting polynomial was obtained using 25 data points centered at the points of interest and the data step size was 5 meV. The E_1 (3.34 eV), and E_2-E_4 (3.92, 4.49, and 4.97 eV) features were found to be similar to the three-dimensional M_1, and the zinc-blende E_2-type critical-point contributions in III–V compounds, respectively. These individual contributions were modeled by particular expressions

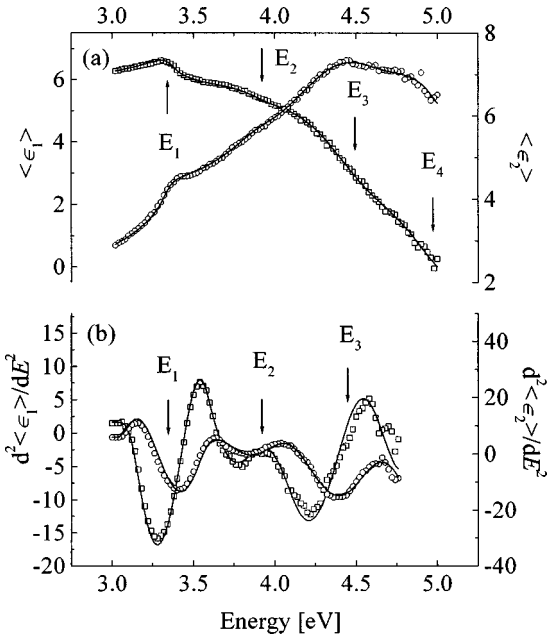

FIG. 5. Experimental data (□ real part, ○ imaginary part) for the pseudodielectric function $\langle\epsilon\rangle$ (a), and its second derivative $d^2\langle\epsilon\rangle/dE^2$ (b). The experimental data were obtained by averaging the reflection gVASE data R_{pp} acquired at multiple sample azimuths because no measurable anisotropy could be detected ($R_{sp}=R_{ps}=0$). The gVASE data are identical to the standard ellipsometric parameters Ψ and Δ, which are then converted to $\langle\epsilon\rangle$ (Ref. 17). The arrows show direct band-to-band transitions identified through modeling the dispersion of ϵ (corrected for surface roughness as described in the text) by one three-dimensional M_1-type (E_1) and three damped harmonic oscillator (E_2–E_4) contributions to the bulk dielectric function of our $CdAl_2Se_4$ sample (Table II) after Adachi (Ref. 25, solid lines). Note that due to the limitation of the spectral range investigated, the second derivative does not include the E_4 critical-point contribution.

for ϵ given in Ref. 29. The results from the best fit for the critical-point parameters are given in Table II. Note that the E_2-type transitions (E_2–E_4) were characterized by damped harmonic oscillators (DHO's). A surface roughness layer ($d_r=70\pm5$ nm) was modeled during the same regression analysis through an effective medium approximation by equally weighing the unity (air, $n=1$) and $CdAl_2Se_4$ dielectric function.[28] In order to account for higher-order transitions we considered an additional term, $\epsilon_{1\infty}$, to ϵ. This term is assumed to have slight dispersion, and was modeled by an undamped harmonic oscillator (HO, Table II). Note that due to the limitation of the spectral range investigated and the necessity of surrounding data points for numerical evaluation of $d^2\langle\epsilon\rangle/dE^2$ the E_4 critical-point contribution is not included in Fig. 5(b). Note finally that we could not resolve spin-orbit splittings. Also, the data did not contain sensitivity to determine excitonic contributions to the critical-point structures.

TABLE II. Best fit of critical-point (CP) parameters of $CdAl_2Se_4$ to the reflection-type data employing Adachi's semiconductor compound CP model (Ref. 25).

CP structure ν	CP model type	A_ν	E_ν (eV)	Γ_ν (eV)
1	3D-M_1[a]	0.38	3.36	0.039
2	DHO[b]	0.04	3.93	0.099
3	DHO	0.67	4.51	0.155
4	DHO	1.65	4.98	0.158
5	HO	2.34	6.62	0[c]

[a] $\epsilon_\nu(E)=-A_\nu\chi_\nu^{-2}\ln(1-\chi_\nu^2)$, $\chi_\nu=(E+i\Gamma_\nu)/E_\nu$ (Ref. 29).
[b] $\epsilon_\nu(E)=A_\nu/[1-(E/E_\nu)^2-i\Gamma E/E_\nu]$ (Ref. 29).
[c] Undamped harmonic oscillator to account for higher-order transition contributions to $\epsilon_{1\infty}$.

IV. SUMMARY

An anisotropy ellipsometry technique has been used to characterize the optical properties of a single-crystal $CdAl_2Se_4$ sample grown by the chemical vapor transport method. Reflection- and transmission-type data were taken in the spectral range from 0.74 to 5 eV. From the analysis of the transmission-type data below the band gap we obtain the uniaxial major refractive indices, the major crystal axis orientations, and the thickness of the sample. The onset of absorption implies the fundamental band edge E_0 at $\sim$2.95 eV. However, the nature of the lowest transition observed here remains unresolved. No anisotropy was observed in the reflection-type data above the fundamental band edge (3–5 eV) which is interpreted as being due to the polishing process in which crystallographic defects are incorporated into the near-surface region. From a line-shape analysis of the pseudodielectric function and its second derivative above the fundamental band edge we assign four possible critical point contributions (E_1–E_4). The band-to-band transitions were identified by modeling the dispersion of the $CdAl_2Se_4$ dielectric function using one three-dimensional M_1-type ($E_1=3.34$ eV), and three zinc-blende E_2-like ($E_2=3.92$ eV, $E_3=4.49$ eV, and $E_4=4.97$ eV) critical points.

ACKNOWLEDGMENTS

The authors are indebted to C. M. Herzinger, J. A. Woollam Co., for supplying the numerical procedures for the treatment of multibeam propagation in biaxial substrates. We thank Professor R. Schwabe and Professor K. Kreher for useful discussions. We further wish to acknowledge T. Saß, G. Lippold, B. Rheinländer, and H.-J. vom Hofe for helpful comments and sample preparation. The research described in this paper was made possible by the Deutsche Forschungsgemeinschaft under Grant No. Ri756/1-3 and Rh28/1-1.

*Electronic address: hecht@aix550.informatik.uni-leipzig.de

[1] J. L. Shay and J. H. Wernick, *Ternary Chalcopyrite Semiconductors: Growth, Electronic Properties, and Applications* (Pergamon, Oxford, 1975).

[2] T. J. Coutts, L. U. Kazmerski, and S. Wagner, *Copper Indium Diselenide for Photovoltaic Applications* (Elsevier, Amsterdam, 1986).

[3] M. A. Gabor, J. R. Tuttle, D. S. Albin, M. A. Contreras, R. Noufi, and A. M. Hermann, Appl. Phys. Lett. **65**, 198 (1994).

[4] *Proceedings of the 12th European Photovoltaic Energy Confer-*

ence, edited by R. Hill, W. Palz, and P. Helm (Stephens & Associates, Amsterdam, 1994).
[5] G. Krauss, V. Krämer, A. Eifler, V. Riede, and S. Wenger, Cryst. Res. Technol. **32**, 223 (1997).
[6] A. Baldereschi, F. Meloni, F. Aymerich, and G. Mula, Solid State Commun. **21**, 113 (1977).
[7] F. Meloni, F. Aymerich, G. Mula, and A. Baldereschi, Helv. Phys. Acta **49**, 687 (1976).
[8] A. MacKinnon, Jpn. J. Appl. Phys. **19**, 157 (1980).
[9] J. E. Bernard and A. Zunger, Phys. Rev. B **37**, 6835 (1988).
[10] R. Trykozko and D. Huffman, J. Appl. Phys. **52**, 5283 (1981).
[11] N. N. Syrbu and V. E. Tezlevan, Physica B **210**, 43 (1995).
[12] R. M. A. Azzam and N. M. Bashara, *Ellipsometry and Polarized Light* (North-Holland, Amsterdam, 1984).
[13] M. Schubert, B. Rheinländer, J. A. Woollam, B. Johs, and C. M. Herzinger, J. Opt. Soc. Am. A **13**, 875 (1996).
[14] M. Schubert, B. Rheinländer, C. Cramer, H. Schmiedel, C. M. Herzinger, B. Johs, and J. A. Woollam, J. Opt. Soc. Am. A **13**, 1930 (1996).
[15] M. Schubert, B. Rheinländer, E. Franke, H. Neumann, J. Hahn, M. Röder, and F. Richter, Appl. Phys. Lett. **70**, 1819 (1997).
[16] M. Schubert, Phys. Rev. B **53**, 4265 (1996).
[17] G. E. Jellison, Thin Solid Films **234**, 416 (1993).
[18] J. F. Elman, J. Greener, C. M. Herzinger, and B. Johs, Thin Solid Films (to be published).
[19] S. Zollner, Appl. Phys. Lett. **63**, 2523 (1993).
[20] C. M. Herzinger, H. Yao, P. G. Snyder, F. G. Celii, Y.-C. Kao, B. Johs, and J. A. Woollam, J. Appl. Phys. **77**, 4677 (1995).
[21] C. C. Kim, J. W. Garland, H. Abad, and P. M. Raccah, Phys. Rev. B **45**, 11 749 (1992).
[22] C. C. Kim, J. W. Garland, and P. M. Raccah, Phys. Rev. B **47**, 1876 (1993).
[23] J. W. Garland, C. Kim, H. Abad, and P. M. Raccah, Phys. Rev. B **41**, 7602 (1990).
[24] A. Savitzky and M. J. E. Golay, Anal. Chem. **36**, 1627 (1964).
[25] S. Adachi, Phys. Rev. B **35**, 7454 (1987).
[26] *Guide to Using WVASE32* (Woollam, Lincoln, 1995), pp. 216–217.
[27] D. E. Aspnes and A. A. Studna, Phys. Rev. B **27**, 985 (1983).
[28] D. E. Aspnes and J. B. Theeten, Phys. Rev. B **20**, 3292 (1979).
[29] S. Ozaki, S. Adachi, M. Sato, and K. Ohtsuka, J. Appl. Phys. **79**, 439 (1996).